A realistic coupled nonlinear artificial ECG, BP and respiratory signal generator for assessing noise performance of biomedical signal processing algorithms

Gari D. Clifford[a] and Patrick E. McSharry[b]

[a]Harvard-MIT Division of Health Sciences, 45 Carleton St., Cambridge MA 02142, US.
[b]Department of Engineering Science, University of Oxford, Parks Road, Oxford OX1 3PJ, UK;

ABSTRACT

Extensions to a previously published nonlinear model for generating realistic artificial electrocardiograms to include blood pressure and respiratory signals are presented. The model accurately reproduces many of the important clinical qualities of these signals such as QT dispersion, realistic beat to beat variability in timing and morphology and pulse transit time.

The advantage of this artificial model is that the signal is completely known (and therefore its clinical descriptors can be specified exactly) and contains no noise. Artifact and noise can therefore be added in a quantifiable and controlled manner in order to test relevant biomedical signal processing algorithms. Application examples using Independent Component Analysis to remove artifacts are presented.

Keywords: Electrocardiogram, blood pressure, artificial signal, independent component analysis, noise, measurement error, EKG, respiration, nonlinear model, noise removal

1. INTRODUCTION

In an earlier publication[1] the authors demonstrated how a dynamical model based on three coupled ordinary differential equations is capable of generating realistic synthetic electrocardiograms (ECGs). Open source code for this model is freely available from Physionet[2] in C, Matlab and Java programming languages. This article demonstrates how the same model can be used to generate realistic blood pressure (BP) and respiration signals with realistic inter-signal coupling between the respiration, BP and ECG time series.

The time-varying surface ECG reflects the ionic current flow which causes the cardiac fibers to contract and subsequently relax. A single normal (sinus) cycle of the ECG represents the successive atrial depolarization/repolarization and ventricular depolarization/repolarization which occurs with every heart beat. These can be approximately associated with the peaks and troughs of the ECG waveform labeled P,Q,R,S and T as shown in Fig. 1a. The RR-interval is the time between successive R-peaks, the inverse of this time interval gives the instantaneous heart rate, HR_i. The current model exhibits realistic changes in RR-intervals, R-peak amplitudes and QT-intervals.

After the R-peak on the ECG there is a short delay, known as the Left Ventricular Ejection Time (LVET), before the blood volume is pushed out of the left ventricle and into the arterial system. By placing a recording device in or near the arterial tree (such as a catheter or photoplethysmogrphy device), a pulsatile waveform may be measured that represents the blood flow over time. Fig. 1b illustrates the salient features of such a waveform. The four main points that are labeled are the systolic BP at the onset of the waveform (Q), the diastolic BP at the peak of the waveform, (R), the cusp of the dialstoic reflected wave* (S), and the waveform offset (T). The Pulse Transmission Time (PTT) is taken to be the time difference between the ECG R-peak and the onset of the BP waveform; $t_R^{ECG} - t_Q^{BP}$.

Further author information: (Send correspondence to Gari D. Clifford)
Gari D. Clifford.: E-mail: gari@mit.edu, Telephone: +1 617 452 2575
Patrick E. McSharry: E-mail: patrick@mcsharry.net, Telephone: +44 1865 273096

*DRW - sometimes erroneously mistaken for the *dichrotic notch*
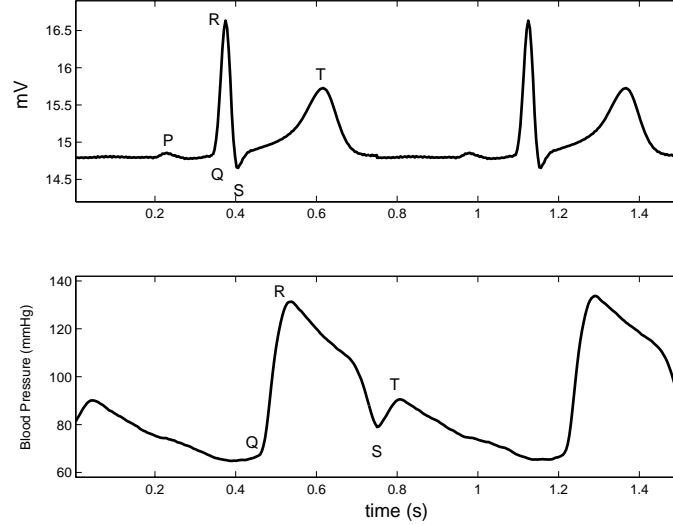
Figure 1. Upper plot (a) - Morphology of a mean PQRST-complex of an ECG recorded from a normal human. Lower plot (b) - Real BP waveform - from Physionet mghdb[4]; subject mgh0007.

Table 1. Parameters of the ECG model given by (1)

Index (i)	P^{ECG}	Q^{ECG}	R^{ECG}	S^{ECG}	T^{ECG}
Time (secs)	-0.2	-0.05	0	0.05	0.3
θ_i (radians)	$-\frac{1}{3}\pi$	$-\frac{1}{12}\pi$	0	$\frac{1}{12}\pi$	$\frac{1}{2}\pi$
a_i	1.2	-5.0	30.0	-7.5	0.75
b_i	0.25	0.1	0.1	0.1	0.4

Extracting useful clinical information from the real (noisy) ECG and BP signals requires reliable signal processing techniques These include peak detection pulse and QT-interval detection and the derivation of heart rate and respiration rate from these signals.[3] For example, the variability of a series of peak-to-peak waveform intervals (known as a RR tachogram on the ECG) is understood to reveal important information about the physiological state of a subject.[3] At present, new biomedical signal processing algorithms are usually evaluated by applying them to signals in a large database such as the Physionet database.[4] While this gives the operator an indication of the accuracy of a given algorithm when applied to real data, it is difficult to infer how the performance would vary in different clinical settings with a range of noise levels and sampling frequencies. Having access to realistic artificial biomedical signals may facilitate this evaluation.

This paper presents a method for augmenting the existing ECG model to generate a multiparameter synthetic biomedical signal generator capable of generating realistic ECG, BP and respiration with their associated couplings. The aim of this model is to provide standard realistic biomedical signals with known characteristics, which can be generated with specific statistics such as the mean and standard deviation of the heart rate and frequency-domain characteristics of heart rate variability (HRV),[3] and at different sampling frequencies with different noise levels. This may enable clinicians to ascertain which biomedical signal processing techniques were best for a given application. As an illustration, the performance of ICA in removing noise from the ECG and BP signals is studied.
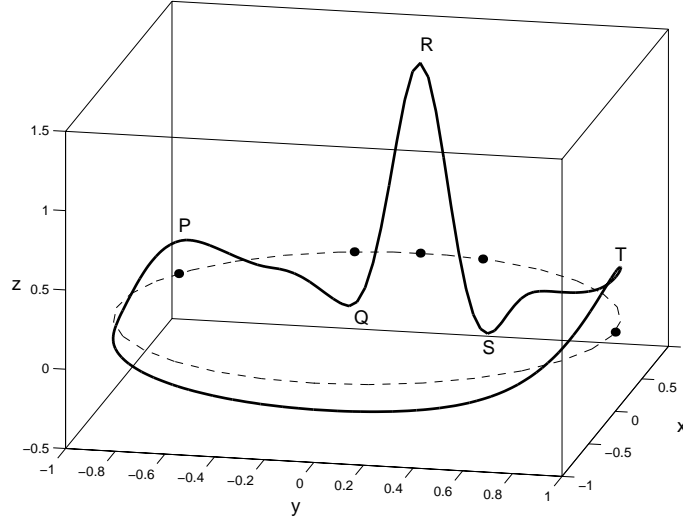
Figure 2. A typical trajectory generated by the dynamical model (1) in the three-dimensional space given by (x, y, z). The dashed line reflects the limit cycle of unit radius while the small circles show the positions of the P,Q,R,S,T events.
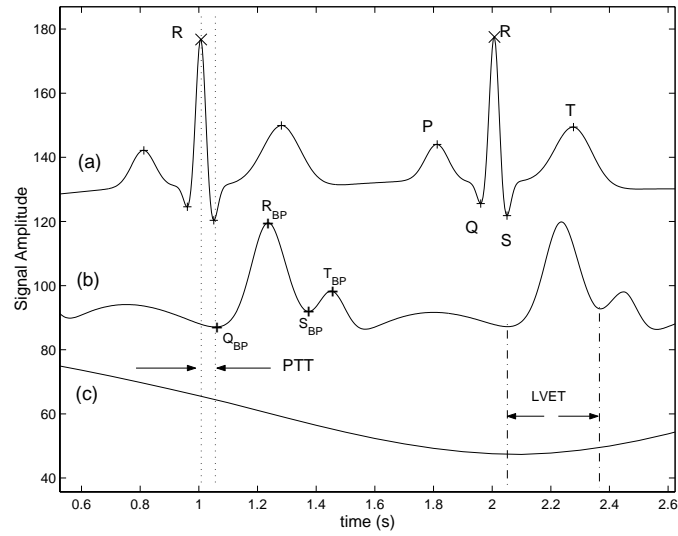
Figure 3. ECG (a), BP (b), and respiratory (c) signals labeled with pulse transmission time (PTT), left ventricular ejection time (LVET) and important markers (P, Q, R, S, and T). Generated by integrating equation (1) over the parameters in Tables 1 and 2.

Table 2. Parameters of the BP model for equation (1)

Index (i)	P^{BP}	Q^{BP}	R^{BP}	S^{BP}	T^{BP}
Time (secs)	0.21	0.01	0	0.03	0.22
θ_i (radians)	$-\frac{5}{12}\pi$	$-\frac{1}{36}\pi$	0	$\frac{1}{18}\pi$	$\frac{4}{9}\pi$
a_i	0	0	0.45	0.25	0.45
b_i	0.25	0.1	0.3	0.5	0.3
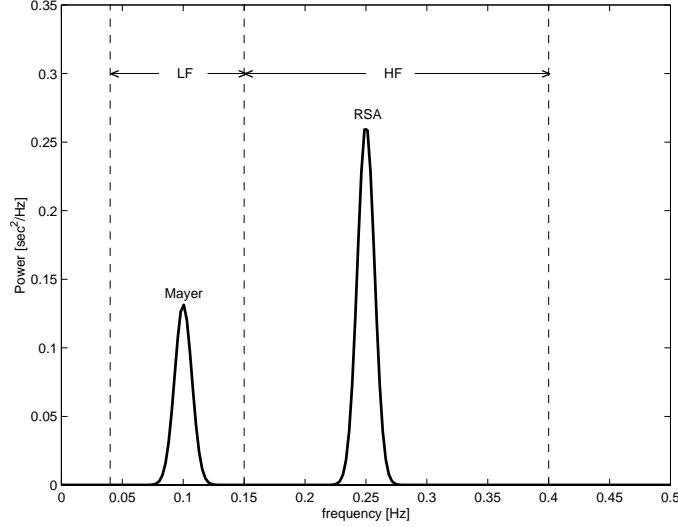
Figure 4. Power spectrum $S(f)$ of the RR-interval process with a LF/HF ratio of $\sigma_1^2/\sigma_2^2 = 0.5$.

2. METHODS

2.1. The dynamical model

The model generates a trajectory in a three-dimensional state space with co-ordinates (x, y, z). Quasi-periodicity of the ECG is reflected by the movement of the trajectory around an attracting limit cycle of unit radius in the (x, y)-plane. Each revolution on this circle corresponds to one RR-interval or heart beat. Inter-beat variation in the ECG is reproduced using the motion of the trajectory in the z-direction. Distinct points on the ECG, such as the P,Q,R,S and T are described by *events* corresponding to negative and positive extrema in the z-direction. These events are placed at fixed angles around the unit circle given by θ_P, θ_Q, θ_R, θ_S and θ_T (see Fig. 2). When the trajectory approaches one of these events, it is pushed upwards or downwards away from the limit cycle, and then as it moves away it is pulled back towards the limit cycle.

The dynamical equations of motion are given by a set of three ordinary differential equations

$$
\begin{aligned}
\dot{x} &= \alpha x - \omega y, \\
\dot{y} &= \alpha y + \omega x, \\
\dot{z} &= -\sum_{i \in \{P,Q,R,S,T\}} a_i \Delta\theta_i \exp(-\Delta\theta_i^2/2b_i^2) - (z - z_0),
\end{aligned}
\tag{1}
$$

where $\alpha = 1 - \sqrt{x^2 + y^2}$, $\Delta\theta_i = (\theta - \theta_i) \bmod 2\pi$, $\theta = \text{atan2}(y, x)$ and ω is the angular velocity of the trajectory as it moves around the limit cycle. Baseline wander is introduced by coupling the baseline value z_0 in (1) to the respiratory frequency f_2 using

$$
z_0(t) = A \sin(2\pi f_2 t),
\tag{2}
$$

where $A = 0.15$ mV.

These equations of motion given by (1) were integrated numerically using a fourth order Runge-Kutta method[5] with a time step $\Delta t = 1/f_{int}$ where f_{int} is the internal sampling frequency and must be an integer multiple of the output sampling frequency f_s. Experiments have shown that if either f_s or $f_{int} << 512$Hz then serious errors may result.[6]

Visual analysis of a section of typical ECG from a normal subject was used to suggest suitable times (and therefore angles θ_i) and values of a_i and b_i for the PQRST points. The times and angles are specified relative to the position of the R-peak and are detailed in Table 1.

A trajectory generated by integrating equation (1) in three-dimensions corresponding to (x, y, z) is illustrated in Fig. 2. This demonstrates how the positions of the events P, Q, R, S, T act on the trajectory in the z-direction as it precesses around the unit circle in the (x, y)-plane. The z variable from the three-dimensional system (1) yields a synthetic ECG with realistic PQRST morphology (Fig. 3a). The similarity between the synthetic ECG and the real ECG may be seen by comparing Fig. 3a with Fig. 1a. Note that noise has not been added to the model at this point.

By contrasting the dynamical model (1) with the mechanisms underlying the cardiac cycle, it is obvious that the time required to complete one lap of the limit cycle is equal to the RR-interval of the synthetic ECG signal. Variations in the length of the RR-intervals can be incorporated by varying the angular velocity ω.

2.2. Adding best-to-beat variability

Analysis of variations in the instantaneous heart rate time series using the beat-to-beat RR-intervals (the RR tachogram) is known as Heart Rate Variability (HRV) analysis.[3] HRV analysis has been shown to provide an assessment of cardiovascular disease.[7] The heart rate may be increased by slow acting sympathetic activity or decreased by fast acting parasympathetic (vagal) activity. The balance between the effects of the sympathetic and parasympathetic systems, the two opposite acting branches of the autonomic nervous system, is referred to as the sympathovagal balance and is believed to be reflected in the beat-to-beat changes of the cardiac cycle.[3] The heart rate is given by the reciprocal of the RR-interval in units of beats per minute. Spectral analysis of the RR tachogram is typically used to estimate the effect of the sympathetic and parasympathetic modulation of the RR-intervals. The two main frequency bands of interest are referred to as the Low-Frequency (LF) band (0.04 to 0.15 Hz) and the High-Frequency (HF) band (0.15 to 0.4 Hz) which are believed to mostly reflect the subject's sympathetic and parasympathetic activity.[3]

Respiratory Sinus Arrhythmia (RSA)[8,9] is the name given to the oscillation in the RR tachogram due to parasympathetic activity which is synchronous with the respiratory cycle. The RSA oscillation manifests itself as a peak in the HF band of the spectrum. For example, 15 breaths per minute corresponds to a 4 second oscillation with a peak in the power spectrum at 0.25 Hz. A second peak is often found in the LF band of the spectrum at approximately 0.1 Hz. While the cause of this 10 second rhythm is strongly debated, one possible explanation is that it may be due to baroreflex regulation which creates the so-called *Mayer waves* in the blood pressure signal.[10] The effects of both RSA and Mayer waves in the power spectrum $S(f)$ of the RR-intervals are incorporated by generating RR-intervals which have a bimodal power spectrum consisting of the sum of two Gaussian distributions,

$$S(f) = \frac{\sigma_1^2}{\sqrt{2\pi c_1^2}} \exp\left(\frac{(f - f_1)^2}{2c_1^2}\right) + \frac{\sigma_2^2}{\sqrt{2\pi c_2^2}} \exp\left(\frac{(f - f_2)^2}{2c_2^2}\right), \tag{3}$$

with means f_1, f_2 and standard deviations c_1, c_2. Power in the LF and HF bands are given by σ_1^2 and σ_2^2 respectively whereas the variance equals the total area $\sigma^2 = \sigma_1^2 + \sigma_2^2$, yielding an LF/HF ratio of σ_1^2/σ_2^2. Fig. 4 shows the power spectrum $S(f)$ given by $f_1 = 0.1$, $f_2 = 0.25$, $c_1 = 0.01$, $c_2 = 0.01$ and $\sigma_1^2/\sigma_2^2 = 0.5$. The Gaussian frequency distribution is motivated by the typical power spectrum of a real RR tachogram.[3]

A RR-interval time series $T(t)$ with power spectrum $S(f)$ is generated by taking the inverse Fourier transform of a sequence of complex numbers with amplitudes $\sqrt{S(f)}$ and phases which are randomly distributed between 0 and 2π. By multiplying this time series by an appropriate scaling constant and adding an offset value, the resulting time series can be given any required mean and standard deviation. The time-dependent angular velocity $\omega(t)$ of motion around the limit cycle is then given by $\omega(t) = 2\pi/T(t)$. In this way the series of RR-intervals of the resultant synthetic ECG will also have a power spectrum equal to $S(f)$; this will be demonstrated in the next section.

2.3. Generating the respiratory signal

It can be seen from equation (3) that the second term generates the oscillations in the RR intervals due to respiration. Therefore the inverse Fourier transform of this second term is used to generate the respiratory signal, which is them resampled to 10Hz (well above the Nyquist criterion even for hyperventilation). Figure 5b
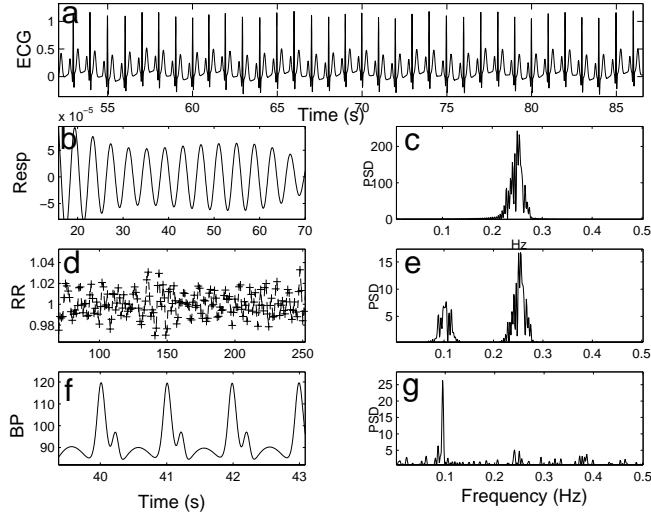
Figure 5. ECG (a), respiration (b) with corresponding PSD (c), RR intervals (d) with corresponding PSD (e) and BP (f) with corresponding PSD derived from peak height oscillations (g). All signals were generated from 1, 3 and 2 using parameters from Tables 1 and 2.

illustrates an instance of this signal and Figure 5c illustrates its power spectral density (PSD). Note the strong correspondence between the respiratory PSD peak and the peak in the HF region of the RR-interval PSD.

Investigations of the phase relationship between respiration and the RR interval variation indicate that the angle is a function of patient activity and physical fitness.[11] A definite phase difference is therefore not set and instead the phase relationship between the respiration and the RR intervals, ϕ_{r-rr}, as a free parameter to be set by the user. Examples of the respiratory waveform are given in Figures 3c and 5b.

3. EXTENDING THE MODEL FOR BLOOD PRESSURE WAVEFORMS

In order to generate realistic BP waveforms, in isolation from the ECG, it is simply a matter of adjusting the θ_i, a_i and b_i until a realistic waveform results. Table 2 presents an example of such a set of parameters, which are used throughout this paper. Note that a_P and a_Q have been set to zero to push the z-component towards the baseline between beats. θ_Q therefore occurs at the foot of the BP upstroke, the accepted fiducial marker for the pulsatile BP waveform. Figure 3b illustrates the morphology that results from these parameters. Note the salient waveform features; the rise onset, the crest of the largest of the two peaks of each waveform, the cusp between the two peaks (the DRW) and the crest of the second, smaller peak. Each of these are denoted Q, R, S, T respectively in the model and correspond to the analogous extrema θ_i^{ECG} in the ECG model.

The beat to beat variations in timing and shape of the pulsatile BP waveform therefore result from the changes in angular frequency in the (x, y) plane (driven by the RR interval time series) in the same manner as for the ECG. In particular, a lower heart rate (higher RR interval) leads to a broadening wave, which is associated with a longer left ventricular ejection time (LVET),[12] the time between the opening and the closing of the aortic valve. It should be noted that the pre-ejection period, the time during which the left ventricle generates enough force to eject the blood (measured from the onset of ventricular depolarization to the opening of the aortic valve) is often difficult to measure and has therefore not been incorporated into the model.

3.1. BP-ECG relationships

The time interval between the ejection of blood from the heart (roughly corresponding to the peak of the R-wave on the ECG) to the onset of the pulsatile BP waveform is known as the pulse transmission time (PTT) and is equal to $60/\mathrm{HR}_i(\theta_Q^{BP} - \theta_R^{ECG})$ seconds in the model. Figure 3 illustrates this interval. PTT is inversely related to

the pulse wave velocity down the artery which is known to be influenced by the arterial compliance (often related to age), BP and HR.[13, 14] The model does not consider the effect of arterial compliance since the intention is not to model the interaction of the electrophysiology and hemodynamics of the cardiovascular system, but rather to provide a realistic waveform generator to assess signal processing techniques. However, changes in PTT and BP as a function of heart rate or RR interval are incorporated.

Drinnan et $al.$[14] have demonstrated that there is a strong correlation (C=0.7) between PTT and RR interval. The θ_i^{BP} is therefore pre-multiplied by a factor proportional to $1/HR_{mean}$, causing a decreasing delay between the θ_i^{ECG} and the θ_i^{BP} for increasing mean heart rates. It is generally accepted that as BP falls, tension in the arterial wall falls and the PTT increases; and vice versa.[15] The systolic (peak) BP is therefore linearly coupled to mean heart rate (and hence inversely to the PTT). It should be noted that these changes are not always in phase with the exact delay depending upon the physiological state.[11, 16] For instance, the work of DeBoer[10] and more recently Cavalcanti et $al.$[17] indicate that intra-thoracic pressure changes from respiration result in changes in BP which in turn lead to HR changes. However, Drinnan et $al.$[14] and Zhao et $al.$[18] have observed that (paced) respiration changes drive RR interval changes which, after two or three beats lead to PTT and BP changes. Others[11, 16] have shown that phase locking can occur with changes in respiration, HR and BP occurring in phase. This latter (and more simple) option has therefore been adopted. The exact delay is chosen in line with the measurements of Drinnan et $al.$[14] where PTT changes from 7 to 23 ms equate with RR interval changes from between 86 to 443 ms.

Chirife et $al.$[19] has show that the LVET is related to the time between the onset of the BP waveform and the DRW (the points θ_Q^{BP} and θ_S^{BP} - see figure 3b). The LVET has been shown to be longer for lower HR[12] which manifests naturally in the model since the slowing of the HR (lengthening of the RR interval resulting in a lower angular velocity, ω, in the (x, y) plane) leads to a lengthening (in time) of the trajectory between the θ_i .

4. AN APPLICATION: NOISE REDUCTION USING ICA

In order to analyse each single channel of data separately the method of Broomhead and King[20] is used, who introduced singular value decomposition (SVD) in combination with Takens' theorem[21] of time-delay embeddings (which states that it should be possible to reconstruct the dynamics of a deterministic system). The method involves projecting each sample y_t, which is the observable signal representing the state of the system $Y(t)$, onto the feature space. In this space each delay vector, $\mathbf{Y_i}$, contains a section of time series data containing m samples, sampled with a delay, or lag, of τ_s samples between each successive sample. Therefore each delay vector is a point in the embedding space $\mathbf{R}^m$ and represents a window of data, of length m, of the time series. To construct the embedding matrix $\mathbf{Y}$ that represents a discrete trajectory of the ECG data through a certain period of time, this window is passed over a section of data constructing n successive delay vectors that correspond to the columns of the embedding matrix that map out this trajectory. Therefore the observed ECG signal, $y_i = y(i\tau_s)$ is transformed into an $m \times n$ matrix,

$$\mathbf{Y} = \begin{bmatrix} y_1 & y_{1+\tau_s} & \cdots & y_{1+(n-1)\tau_s} \\ y_{1+\tau_s} & y_{2+2\tau_s} & \cdots & y_{1+n\tau_s} \\ \vdots & \vdots & & \vdots \\ y_{1+(m-1)\tau_s} & y_{2+m\tau_s} & \cdots & y_{1+(m+n-2)\tau_s} \end{bmatrix} \tag{4}$$

The traditional assumption that there exists an orthogonal set of vectors spanning the feature space means that SVD can be used to calculate the eigenvectors and eigenvalues of the transformation described by the embedding matrix, $\mathbf{Y}$. Consider the real $m \times n$ matrix $\mathbf{Y}$ which may be decomposed as follows;

$$\mathbf{Y} = \mathbf{U} * \mathbf{S} * \mathbf{V^T} \tag{5}$$

where S is a diagonal matrix of singular values (the singular spectrum) whose elements are arranged in descending order of magnitude. The columns of V are the eigenvectors of $\mathbf{P} = \mathbf{Y} * \mathbf{Y^T}$ and the matrix U is the matrix of projections of $\mathbf{Y}$ onto the eigenvectors of $\mathbf{P}$.[22] If a truncated SVD of $\mathbf{Y}$ is performed (using the most significant p eigenvectors, then the SVD $cleaned$ signal is given by $\mathbf{Z} = \mathbf{U}\mathbf{U^T}\mathbf{Y^T}$ and first column of the $p \times n$ matrix $\mathbf{Z}$ is the noise reduced signal.
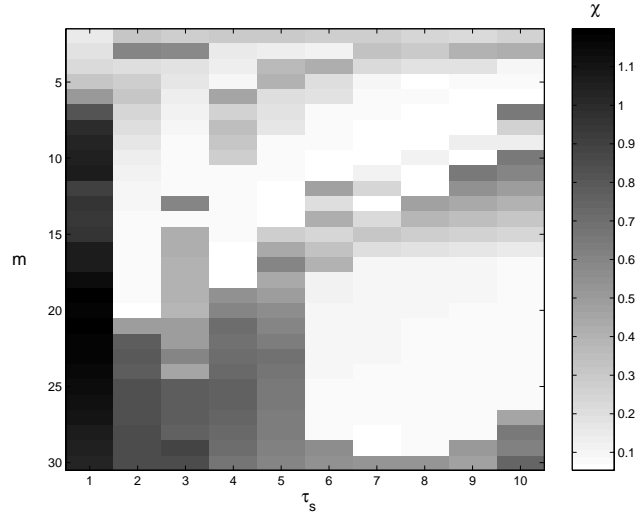
Figure 6. Noise reduction factor χ, over embedding dimensions m and sample delays τ_s for embedding-ICA on noisy artificial ECG.

Although SVD noise reduction performs well when the signals to be separated are orthogonal, (such as Gaussian noise and ECGs), for non-orthogonal signals (such as artifacts on the ECG), more promise has been shown using the well studied method of independent component analysis (ICA).[23–25] Now consider $\mathbf{Y}$ to be a matrix of k observed random vectors, $\mathbf{B}$ a $k \times l$ mixing matrix and $\mathbf{X}$, the l (assumed) source vectors such that

$$\mathbf{Y} = \mathbf{BX} \tag{6}$$

ICA algorithms attempt to find a separating or de-mixing matrix $\mathbf{W}$ such that

$$\mathbf{X} = \mathbf{WY} \tag{7}$$

In practice, iterative methods are used to maximise or minimise a given cost function such as mutual information, entropy or the kurtosis (the fourth order cumulant), which is given by $kurt(\mathbf{y}) = \mathbf{E\{y^4\}} - \mathbf{3(E\{y^2\})^2}$ where $E\{\mathbf{y}\}$ is the expectation of the vector $\mathbf{y}$, a column of $\mathbf{Y}$. The chosen method used in this paper is Cardoso's Multidimensional ICA algorithm $jadeR$,[25] which is based upon the joint diagonalization of cumulant matrices, since it combines the benefits of both PCA and ICA to provide a stable deterministic solution. (ICA suffers from a scaling and column ordering problem due to the indeterminacy of the solution to scalar multipliers and column permutations of the mixing matrix).

Most ICA methods assume there are at least as many independent measurement sensors as sources one wishes to separate ($l \leq k$). Following the method of James et $al.$[26] to perform ICA blind source separation with Cardoso's $jadeR$ algorithm of the embedding matrix $\mathbf{Y}$, the assumption of one signal and one noise source is made. To recover the sources $\mathbf{X}$ by projecting out

$$\hat{\mathbf{x}} = [\mathbf{W} * \mathbf{Y}]_{\mathbf{maxC}} \tag{8}$$

where $\hat{\mathbf{x}}$ is the ICA estimate of $\mathbf{x}$ and $[...]_{\mathbf{maxC}}$ denotes the (normalised) vector that maximally correlates with the normalised columns of $\mathbf{x}$. Note that due to the scaling and inversion indeterminacy problem, the actual output is divided by largest element of $\mathbf{x}$ and then selected as the column of $\hat{\mathbf{x}}$ or $-\hat{\mathbf{x}}$ that has the highest correlation with the original (noise-free) signal.
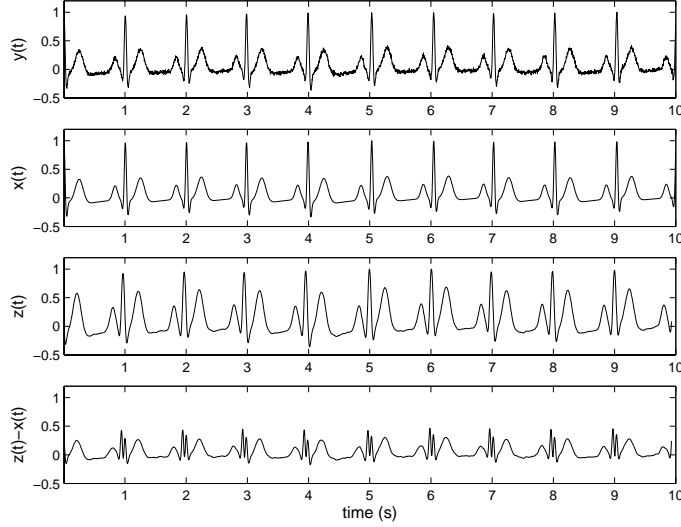
Figure 7. Noisy (observed) ECG, $y(t)$, underlying clean signal, $\mathbf{x(t)}$, optimally cleaned ECG $\mathbf{z(t)}$ from $\mathbf{y(t)}$ using embedding-ICA and error $(\mathbf{z(t)} - \mathbf{x(t)})$.

4.1. Results

In order to determine the optimal delay τ_s and embedding dimension m a measure of how well the signal has been cleaned is required. An intuitive choice is Schreiber and Kaplan's[27] *noise reduction factor*,

$$\chi = \sqrt{\frac{\langle y_i - x_i \rangle^2}{\langle z_i - x_i \rangle^2}} \tag{9}$$

where z_i is the cleaned signal (and equal to $\hat{\mathbf{x}}$ in equation (8)). χ is therefore a measure of the factor by which the RMS error is reduced. Unlike the investigation of Schreiber and Kaplan,[27] the ECG model may be used to obtain a truly noise-free time series x_i so that the value of χ may be viewed as the actual noise reduction factor and not merely a lower bound. The higher the value of χ, the better the noise reduction procedure, whereas $\chi = 1$ indicates no improvement since similar accuracy could have been achieved by using the raw signal, y_i, instead of z_i.

Figure 6 shows the variation in χ for sample delays from 1 to 10 and embedding dimensions from 2 to 30. The darkest region, where $\chi = 1.19$ corresponds to the optimal values of $\tau_s = 1$ sample and $m = 19$. Figure 7 illustrates the noisy signal $\mathbf{y}(t)$, the original underlying signal $\mathbf{x}(t)$, the ICA cleaned signal $\mathbf{z(t)}$, the error between the cleaned signal and the underlying signal $\mathbf{z(t)} - \mathbf{x(t)}$, for these values of τ_s and m. Note that although almost all the Gaussian noise is removed, serious distortion of the ECG actually results with reduced relative R-wave height. This distortion reduces the signal to noise ratio for a QRS detector and will hamper performance, despite the removal of the underlying noise. Note also that the cleaned ECG is delayed with respect to the source and noisy signal due to the embedding process. This offset has been allowed for in calculating χ As expected for Gaussian noise, SVD gave a similar performance to ICA, with a maximal NRF value of $\chi = 1.18$ and Correlation coefficient (between $\mathbf{z}$ and $\mathbf{x}$) of $C = 0.996$ for $m = 19$ and $\tau_s = 1$ using the first five principal components of $\mathbf{Y}$ ($p = 5$). Interestingly, better Gaussian noise reduction was observed in the output signal ($\mathbf{z}$) by using $p = 4$, with $C = 0.994$ and $\chi = 0.89$). However, small distortions in the waveform may lead to small but significant changes in R-peak location, ST-level and QT-interval. Values of $p < 4$ removed all the visible Gaussian noise, but lead to large morphology distortions.

The same experiment was repeated for the artificial BP signal, a 256Hz, 10 second segment ($\mathbf{x(t)}$ in Figure 8). In order to simulate real artifact that might appear on a photoplethismogram, a 4Hz sinusoid, was generated with one tenth the amplitude of the BP signal and a hamming window applied to its length ($\mathbf{e(t)}$ in Figure
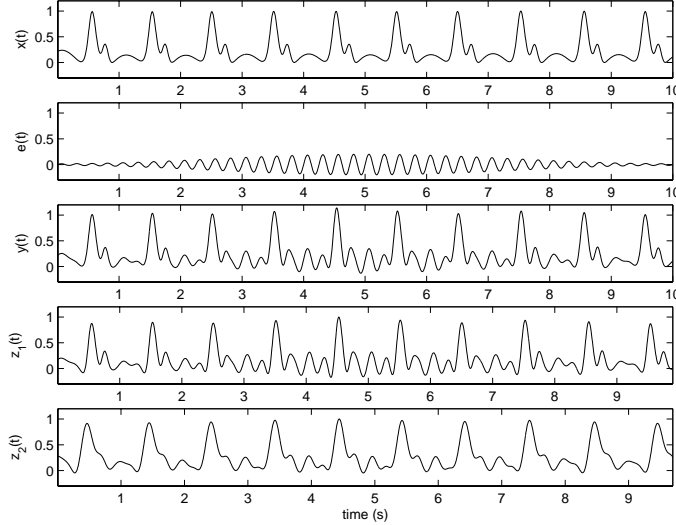
Figure 8. Underlying clean BP signal, $\mathbf{x(t)}$, transient 4Hz sinusoidal noise $e(t)$, noisy (observed) signal $\mathbf{y(t)} = \mathbf{x(t)} + \mathbf{e(t)}$, embedding-ICA cleaned signal, $\mathbf{z_1(t)}$, with largest value of χ and embedding-ICA cleaned signal, $\mathbf{z_2(t)}$, with largest value of C.

8). This is intended to simulate a transient repetitive finger motion, tapping on the sensor. The sum of these two signals ($\mathbf{y(t)} = \mathbf{x(t)} + \mathbf{e(t)}$ in Figure 8) is then evaluated as above. Figure 9a shows the variation in χ for sample delays from 1 to 10 and embedding dimensions from 2 to 70 for this noisy signal. Note that a maximal performance of $\chi = 2.2$ is achieved for $\tau_s = 1$ and $m = 28$. $\mathbf{z_1(t)}$ in Figure 8 is an example of ICA cleaning using these parameters. It can readily be seen that the actual performance for removing the noise from the signal is not as impressive as the χ statistic implies, with an attenuation of only 0.8dB at the frequency of the artifact (4Hz). A better metric for judging noise removal in this case turns out to be a simple correlation C between the original signal and the cleaned signal, with a 2.5dB attenuation at 4Hz. Figure 9b is a greyscale plot of C for the same values of m and τ_s with a maximal value of $C = 0.97$ for $m = 64$ and $\tau_s = 1$.

Note that the correlation between the noisy and original (zero-noise) signal, $\mathbf{x}$, is $C = 0.95$, the same as that between $\mathbf{z_1}$ and $\mathbf{x}$. Note also that the parameters required for largest value of C lead to some distortion of the BP waveform, with a diminished DRW and a broadening of the pulsatile waveform. This would lead to problems with algorithms that relied on detecting the DRW and an over-estimation of the LVET respectively. The parameters required to give the largest value of χ result in little waveform distortion, but no significant noise removal.

Experiments using SVD revealed that this technique is inappropriate for non-Gaussian noise, with maximal values of $\chi = 1.03$ and $C = 0.97$ using $p = 2$. Visual inspection reveals that although $p = 1$ results in a significant reduction in the noise component, the salient features of the signal are heavily distorted.

5. CONCLUSIONS

Extensions to a new dynamical model which is capable of replicating many of the important features present in human ECG, BP and respiratory signals have been introduced. Moreover, many of the morphological changes observed in the human ECG and pulsatile BP waveform manifest as a consequence of the geometrical structure of the model. Model parameters may be chosen to generate varying morphologies for the PQRST waveform. The power spectrum of the RR-intervals can be selected *a priori* and used to generate the respiratory signal and drive the ECG and BP signal generator. This allows the operator to prescribe specific characteristics of the heart rate dynamics such as the mean and standard deviation of the heart rate and spectral properties such as the LF/HF ratio. Key physiological features have been incorporated using motion of a trajectory throughout a three-dimensional state space. The quasi-periodicity of the cardiac cycle is represented by attraction towards a
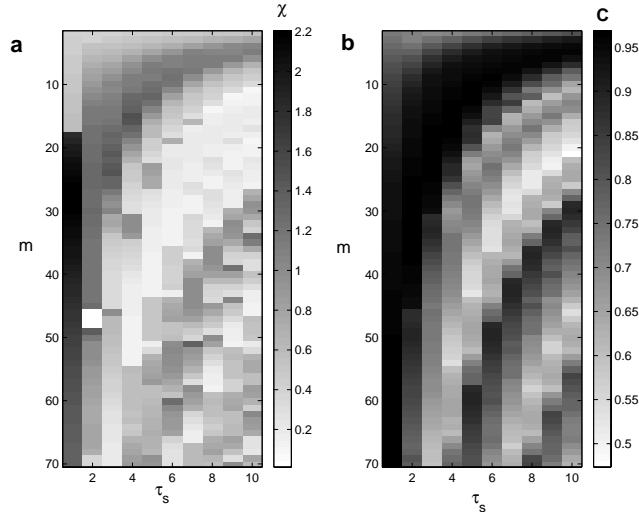
Figure 9. (a) Left: noise reduction factor χ, over embedding dimensions m and sample delays τ_s for embedding-ICA on noisy artificial BP. (b) Right: Correlation of C cleaned signal $\mathbf{z}$, with original signal $\mathbf{x}$, over embedding dimensions m and sample delays τ_s for embedding-ICA on noisy artificial BP.

limit cycle. The model can produce realistic ECGs (with QT-intervals and R-peak height variation (RSA) which vary linearly with the RR-intervals as has been found in real ECGs[28, 29]), blood pressure signals (with correlated LVET and PTT) and respiratory signals (which are couple to both the ECG and BP variations) . Through the application of a modern signal processing technique, ICA,

As an application example, the model is used to assess the noise reduction performance of ICA, which requires perfect knowledge of the underlying signal sources to evaluate the performance correctly. In particular, it is shown that although ICA is an excellent noise removal technique for ECG and BP signals, even with only a single channel, the resultant phase distortion on the ECG and BP signals may introduce significant errors into width or peak location sensitive metrics such as PSD based measures of HRV, ECG-derived respiration, PTT or LVET estimates.

ACKNOWLEDGMENTS

REFERENCES

1. McSharry P.E., Clifford G.D., Tarassenko L., Smith L.: *A dynamical model for generating synthetic electro-cardiogram signals*, IEEE Transactions On Biomedical Engineering, 50(3), 289-294, March 2003.
2. www.physionet.org/physiobank/ecgsyn/
3. Task Force of the European Society of Cardiology, the North American Society of Pacing, and Electrophysiology, "Heart rate variability: standards of measurement, physiological interpretation, and clinical use," 1996.
4. A. L. Goldberger, L. A. N. Amaral, L. Glass, J. M. Hausdorff, P. Ch. Ivanov, R. G. Mark, J. E. Mietus, G. B. Moody, C. K. Peng, and H. E. Stanley, "Physiobank, physiotoolkit, and physionet: Components of a new research resource for complex physiologic signals," *Circulations*, vol. 101, no. 23, pp. e215–e220, 2000.

5. W. H. Press, B. P. Flannery, S. A. Teukolsky, and W. T. Vetterling, *Numerical Recipes in C*, CUP, Cambridge, 2nd edition, 1992.

6. Abboud S., Barnea O.: *Errors due to sampling frequency of electrocardiogram in spectral analysis of heart rate signals with low variability*, Computers in Cardiology, pp 461-463, 1995.

7. M. H. Crawford, S. Bernstein, and P Deedwania, "ACC/AHA guidelines for ambulatory electrocardiography," *Circulation*, vol. 100, pp. 886–893, 1999.

8. S. Hales, *Statical Essays II, Haemastaticks*, Innings and Manby, London, 1733.

9. C. Ludwig, "Beiträge zur Kenntnis des Einflusses der Respirationsbewegung auf den Blutlauf im Aortensystem," *Arch. Anat. Physiol.*, vol. 13, pp. 242–302, 1847.

10. R. W. De Boer, J. M. Karemaker, and J. Strackee, "Hemodynamic fluctuations and baroreflex sensitivity in humans: a beat-to-beat model," *Am. J. Physiol.*, vol. 253, pp. 680–689, 1987.

11. A. Stefanovska, H. Haken, P. V. E. McClintock, M. Hozic, F. Bajrovic, S. Ribaric, *Reversible transitions between synchronization states of the cardiorespiratory system*, Phys. Rev. Lett. 85, 4831-4834, 2000

12. Boudalis H., *Systolic time intervals* in *Cardiac Output Measures*, Robertson JIS & Birkenhager WH (Eds.), Saunders, 1991.

13. Gribbin B, Steptoe A, Sleight P. *Pulse wave velocity as a measure of blood pressure change.* Psychophysiology 1976;13:86-90.

14. . Drinnan M.J., Allen J. and Murray A. *Relation between heart rate and pulse transit time during paced respiration.* Physiol Meas 2001;22:425-32.

15. J R Stradling, C Barbour, J Glennon, B A Langford, and J H Crosby *Which aspects of breathing during sleep influence the overnight fall of blood pressure in a community population?* Thorax, May 1, 2000; 55(5): 393 - 398.

16. Hoyer D., Frasch M.G., Eiselt M., Hoyer O., Zwiener U.: *Validating phase relations between cardiac and breathing cycles during sleep*, IEEE Eng. Med. Biol, March/April 2001.

17. Cavalcanti S.: *Arterial baroreflex influence on heart rate variability: a mathematical model-based analysis*, Med. Biol. Eng. Comput., 38(2): 189-97. Mar 2000.

18. Zhao Y., Yamamoto M., Munakata M., Nakao M. and Kattayama N.: *Investigation of the time delay between variations in heart rate and blood pressure*, Med. Biol. Eng. Comput. 1999;37:344-7.

19. Chirife R., Pigott VM., Spodick DH.: *Measurement of the left ventricular ejection time by digital plethysmography*, American Heart Journal, Aug 1971;Vol 82 No. 2:222-7.

20. Broomhead DS, King GP. *Extracting Qualitative Dynamics from Experimental Data.* Physica D, 20:217-236. 1986.

21. Takens F. *Detecting Strange Attractors in Turbulances.* Lecture Notes in Mathematics, 898:366-381. 1981.

22. Golub, G.H., and Van Loan, C.F.: *Matrix Computations*, 2nd ed. Johns Hopkins Univ. Press, Baltimore 1989.

23. De Lathauwer L., B. De Moor B. and Vandewalle J. *Fetal electrocardiogram extraction by source subspace separation* in Proc. of IEEE Signal Processing / Athos Workshop on Higher-Order Statistics, Girona, Spain, Jun. 1995: 134-138

24. Hyvärinen A, Oja A. *A Fast Fixed Point Algorithm for Independent Component Analysis.* Neural Computation, 9:1483-1492. 1997.

25. Cardoso J-F, *Multidimensional independent component analysis,* Proc. ICASSP'98. Seattle.

26. James CJ and Lowe D. *Extracting multisource brain activity from a single electromagnetic channel*, Artificial Intelligence in Medicine Volume 28, Issue 1 , May 2003, Pages 89-104

27. T. Schreiber and D. Kaplan *Nonlinear noise reduction for electrocardiograms* Chaos **6**(1), pp 87-92, 1996.

28. G. B. Moody, R. G. Mark, M. A. Bump, J. S. Weinstein, A. D. Berman, J. E. Mietus, and A. L. Goldberger, "Clinical validation of the ecg-derived respiration (edr) technique," *Computers in Cardiology*, vol. 13, pp. 507–510, 1986.

29. P. Davey, "A new physiological method for heart rate correction of the QT interval," *Heart*, vol. 82, pp. 183–186, 1999.